Tribology Transactions, 49: 233-247, 2006

ISSN: 1040-2004 print / 1547-357X online
DOI: 10.1080/05698190600614841

The Behavior of Thrust Washer Bearings Considering Mixed Lubrication and Asperity Contact

ROBERT L. JACKSON and ITZHAK GREEN
George W. Woodruff School of Mechanical Engineering
Georgia Institute of Technology
Atlanta, GA 30332-0405

The behavior and life of a tilted flat thrust washer bearing is modeled by a comprehensive numerical code. The goal is to investigate the conditions that distress thrust washer bearings through numerical techniques. The thrust washer bearing supports non-axisymmetric loads within the planetary gear sets of automatic transmissions and consists of flat-faced washers placed between an idle helical gear and its contacting face. Because of non-axisymmetric loading, the gears and washers tilt in relation to the carrier, forming a converging gap that may produce hydrodynamic lift. Various coupled numerical schemes model sliding friction, boundary lubrication, asperity contact, thermo-viscous effects, and full film lubrication. The model provides predictions of frictional torque, bearing temperature, hydrodynamic lift, and other indicators of bearing performance. The results show that the bearing operates in the regimes of boundary lubrication, mixed lubrication, and full-film lubrication, and that the bearing can distress at high loads and speeds.

KEY WORDS

Boundary Lubrication; Hydrodynamic Bearings; Contact of Rough Surfaces

BACKGROUND

The goal of this research is to investigate the physical phenomena that distress a thrust washer bearing system. In one application, the thrust washer bearing system bears the load produced by the planets of a helical planetary gear set within the transmission. The thrust washer bearing system consists of one or two flat-faced washers that are placed between a helical gear and its carrier. From this point forward, "bearing" will refer to the thrust washer bearing system within the test rig, unless specified otherwise. When distress occurs, the planetary gearset locks up and maintenance is required. Experience shows that the failed bearing in the transmission is sometimes completely worn away, thus leaving debris in the transmission fluid. Obviously, this result is undesirable and unacceptable.

**Presented at the STLE Annual Meeting
in Toronto, Ontario, Canada
May 17-20, 2004
Manuscript approved January 4, 2006
Review led by Jane Wang**

To gain an understanding of the bearing behavior under non-axisymmetric loading, a test rig was designed to provide a physical model. The test rig is described in detail in Jackson and Green *(1)*, *(2)*. The test rig controls the operational parameters governing the tribological behavior of the washer. For given washer materials and surface finishes, the parameters that most affect the life of the bearing and its tribological behavior are believed to be thrust or axial load, rotational speed, lubrication supply, lubrication properties, and the geometry of the bearing. The test rig also records pertinent real-time data from the bearing. The frictional torque is recorded from the power output of the motor since, with increasing frictional torque, the power needed to run the motor at a constant speed will increase. The temperatures are recorded using thermocouples embedded near the bearing surface.

In 1958, Cameron and Wood *(3)* formulated a model of a grooved parallel surface thrust bearing, in which the hydrodynamic lift was created by a converging gap induced by thermal deformations. It is noteworthy that in this model the temperature across the fluid film was assumed constant.

More recently, Kazama and Yamaguchi *(4)* modeled a rotating and tilted hydrostatic thrust bearing, including boundary lubrication affects. In many ways, this case is close to the current thrust washer bearing case. The major differences are that they did not account for the effects of frictional heating and there are no hydrostatic pressures in the current case. The Patir and Cheng *(5)*, *(6)* model, which will be discussed in greater detail later, was used to model the mixed lubrication regime.

Groove geometry and thermal effects on the lubrication of thrust washer bearings were studied by Yu and Sadeghi *(7)*, *(8)*. In Yu and Sadeghi *(7)*, *(8)* grooves are the primary means of providing a converging gap capable of causing significant hydrodynamic load carrying capacity. The current study differs since the primary cause for a converging gap to form is the non-axisymmetric loading condition. Kucinschi, et al. *(9)* conduct a similar analysis except thermoelastic deformations are considered. This work (Kucinschi, et al. *(9)*) does not consider asperity contact or boundary lubrication and only models the thrust bearing as having a full film. This and several previous studies state that the grooves allow for the formation of a converging gap by way of thermal deformations, but the grooves can also generate hydrodynamic lift without any thermal deformations. These groove effects will not be present in the current work, although thermal deformations are included.

NOMENCLATURE

B = $0.14\exp(23 \cdot \frac{sy}{E})$ frin fut ub (11)
d = distance between the mean of the surface asperities or peaks
E = elastic modulus
F = force
f = friction coefficient
G_o = Roelands' equation constant
h = film thickness, separation of mean surface height
N = rotational speed in the context of the Stribeck curve
P = contact force or average bearing pressure in the context of the Stribeck curve
p = fluid pressure
p_o = maximum contact pressure
Q = heat rate
q = volumetric heat rate
r = radial distance from axis of symmetry
S_o = Roelands' dquations constant
S_y = yield strength
T = temperature
U = surface tangential speed
x, y, z = Cartesian coordinate system
Z = dynamic viscosity of fluid ($N{\cdot}s/m^2$)

Greek Letters

γ = angle of rotation in thrust washer bearing model
δ = average surface roughness
μ = dynamic fluid viscosity
μ_∞ = Roelands' Equation dynamic fluid viscosity constant
v = Poisson's ratio
Φ_s = stochastic shear flow factor
ϕ = flow factor for modified Reynolds Equation
σ = RMS roughness

Subscripts

1 = surface one
2 = surface two
a = axial
eff = effective
o = maximum or original
s = shear
x = x direction
y = y direction

Also in contrast to the current work that models the thrust washers as free bodies, Kucinschi, et al. and all the previously described works do not. Thus, these investigations are the equivalent of a grooved thrust bearing without any washers.

NUMERICAL MODEL

In conjunction with the experimental effort (see Jackson and Green *(1), (2)*), a numerical simulation of the thrust washer system is constructed herein to provide an analytical model and a better understanding of the washer behavior in order to predict bearing distress. The numerical simulation is also capable of modeling new design concepts to avoid bearing distress. Various mechanical, thermal, and lubrication models are solved simultaneously by using an iterative approach as each of the phenomena is coupled to the other. Upon convergence, the coupled models provide a quasi-steady-state solution. The interfacial conditions between the components, such as fluid pressure and contact force, are adjusted until they converge to the final solution. Although this work primarily addresses the numerical simulation of the thrust washer bearing, the results are also briefly compared to experimental results.

This work outlines the formulation and individual components used in the thrust washer bearing model and then presents the results. The physical mechanisms included in the model are elasto-plastic asperity contact, heat generation and balance, boundary and full-film lubrication, and a force and moment balance. The force and moment balance couples all the effects together through the contact and hydrodynamic pressures. This coupled set of modeled mechanisms effectively results in a group of nonlinear equations that is solved numerically. The following sections detail the modeling techniques used to represent the physical mechanisms.

Assumptions of Numerical Model

The numerical simulation makes several assumptions that may result in differences between the results of the numerical and experimental portions of this investigation. The major assumptions of the model are:

1. In the absence of accurate wear models for lubricated conditions, wear of the component surfaces is excluded. Thus, effects such as wearing-in of the bearing surfaces and dampening are not captured. In other words, the surface topography remains unchanged throughout the simulation. Since currently there are no well-founded wear models to consider (particularly in a lubricated contact), it is neglected.
2. Imperfections in the bearing components such as waviness or large scratches and burrs are not considered. These will vary significantly from sample to sample and so a nominal geometry is used.
3. The model is quasi-steady state and does not consider time-dependent effects such as vibrations and squeeze film effects.
4. The effects of surface and lubricant chemistry at the component interfaces such as oxidation are not considered. In some cases this may be important, but there are no well-founded models to consider this analytically.
5. The gear is held at a constant tilt, which is also the case of the test rig (Jackson and Green *(1), (2)*), used to be obtain the experimental data.
6. The relative speed is prescribed to occur between only two of the thrust washer bearing surfaces. Based on an examination of the wear between experimentally tested washers Jackson and Green *(1), (2)* this also appears to the case during usual operation.
7. Convection is neglected because it is believed to be very small in comparison to the amount of heat conducted away from the bearing.
8. The macro scale deformations of the bearing components are neglected. Once these are considered, it is very difficult to obtain numerical convergence. Most of the hydrodynamic lift is likewise believed to be generated by the tilt of the washers and

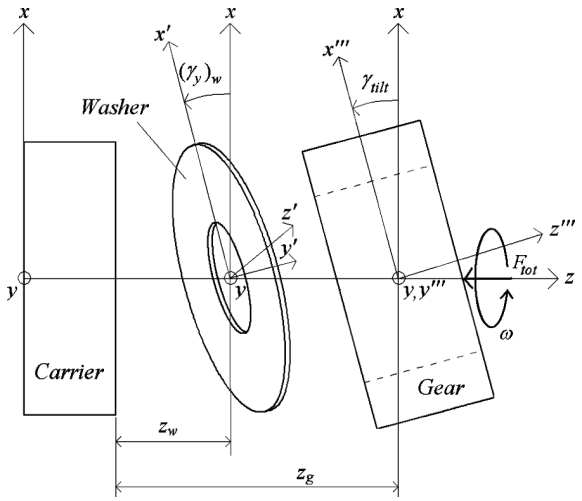

Fig. 1—Diagram of thrust washer bearing testing configuration within the test rig.

not necessarily their deformation. Macroscale washer deformation is a significant undertaking and it is left for future work to investigate such effects.

Figure 1 depicts the one washer bearing assembly looking straight into the y-axis. The gear in the assembly is tilted about the y-axis at an angle, γ_{tilt}. This tilt is held constant and the gear is only allowed to translate along the z-axis (as is indicated by assumption #5). The washer is allowed to tilt (or rotate) about both the x- and y-axis and translate along the z-axis. All of the components will either be in contact, have fluid pressures separating them, or have a combination of both. The location and orientation of each component is determined by solving the set of nonlinear equations resulting from the coupled problem of physical mechanisms outlined in the following sections.

Boundary Lubrication

In regions in or near contact where asperities between surfaces come in close proximity, the asperities can influence the lubrication flow. Here the lubrication regime is known as boundary lubrication; in other words, there is only a thin film of lubricant separating the surfaces, and the micro-topography of the surfaces greatly affects the flow of the lubricant. This work models a thin fluid film between the carrier, washer, and the gear, as shown in Fig. 1.

The ubiquitous Patir and Cheng *(5), (6)* flow factors used in the modified form of the Reynolds equation given by

$$\frac{\partial}{\partial x}\left(\phi_x \frac{h^3}{12\mu}\frac{\partial p}{\partial x}\right)+\frac{\partial}{\partial y}\left(\phi_y \frac{h^3}{12\mu}\frac{\partial p}{\partial y}\right) = \frac{U_1+U_2}{2}\frac{\partial \bar{h}_T}{\partial x}+\frac{U_1-U_2}{2}\sigma\frac{\partial \phi_s}{\partial x}+\frac{\partial \bar{h}_T}{\partial t} \quad [1]$$

where ϕ_x , ϕ_y, and ϕ_s are flow factors that describe the affect the asperities have on the lubricant flow in different directions. Patir and Cheng give formulations for the flow factors as functions of surface roughness, asperity orientation (longitudinal or transverse), and film height. In this work it is assumed that the roughness is isotropic and thus independent of direction. Patir and Cheng's formulations for the flow factors when the roughness is isotropic are:

$$\phi_x = \phi_y = 1 - .90e^{-.56(h/\sigma)} \quad [2]$$

$$\phi_s = \left[\left(\frac{\sigma_1}{\sigma}\right)^2 - \left(\frac{\sigma_2}{\sigma}\right)^2\right]\Phi_s \quad [3]$$

where

$$\Phi_s = 1.899 * (h/\sigma)^{0.98}e^{-0.92h/\sigma+0.05h/\sigma} \quad \text{for} \quad h/\sigma \le 5 \quad [4]$$

$$\Phi_s = 1.126e^{-0.25h/\sigma} \quad \text{for} \quad h/\sigma > 5 \quad [5]$$

where σ_1 and σ_2 are the RMS roughness of each surface and $\sigma = \sqrt{\sigma_1^2 + \sigma_2^2}$. Also, $\bar{h}_T$ is known as the average gap and is defined as

$$\bar{h}_T = \int_{-h}^{\infty}(h+\delta)G(\delta)d\delta \quad [6]$$

where δ is the combined roughness of the two surfaces given by $\delta = \delta_1 + \delta_2$ and G is the Gaussian height distribution of the surface.

In regions where the surfaces are out of the realm of asperity contact ($h/\sigma > 6$) the lubrication model will be solved as a full film automatically by the modified Reynolds equation. This is because as h/σ increases, ϕ_x and ϕ_y approach the value of one and ϕ_s approaches zero so that Eq. [1] reduces to the classic version of the Reynolds equation.

The fluid pressure between the bearing components is solved from the modified Reynolds equation (Eq. [1]). Equation [1] is discretized using a finite difference scheme. The bearing surfaces are meshed by a cylindrical coordinate system. The mesh has 9 nodes in the radial direction and 67 nodes in the circumferential direction. A corresponding film thickness, h, is calculated at each node. At the inner and outer radii of the bearing, the boundary condition $p = 0$ is applied to simulate ambient gauge pressure. Around the circumference of the bearing surface the pressure follows the cyclic boundary condition. To model cavitation of the fluid, the Reynolds boundary condition is assumed. The Gauss-Seidel overrelaxation method is used to iteratively solve the resulting set of equations. The fluid pressure, p, is solved for at each nodal location on the bearing.

The force-balance section of the numerical model requires the fluid force at the nodes on the surface of the bearing rather than values for the average fluid pressure. Linear interpolation is used to predict the pressure distribution between the nodes using the scheme outlined on pages 308-311 of Reddy *(10)*. Then the pressure over the areas surrounding each node are integrated to calculate the force at each node i, giving

$$F^i_{\text{fluid}} = \int_{A_i} p dA_i \quad [7]$$

Elasto-Plastic Asperity Contact

This work uses the statistical elasto-plastic asperity contact model derived in Jackson and Green *(11), (12)* and confirmed for a broad range of material properties by Quicksall, et al. *(13)*. By fitting equations to finite element results, Jackson and Green provide the following equations to predict the elastic-perfectly plastic contact of a sphere and a rigid flat:

For $0 \le \omega^* \le \omega_t^*$

$$\frac{\bar{P}_F}{\bar{P}_c} = \left(\frac{\omega}{\omega_c}\right)^{3/2} \quad [8]$$

For $\omega_t^* \le \omega^*$

$$\frac{\bar{P}_F}{\bar{P}_c} = \left\{\exp\left[-\frac{1}{4}\left(\frac{\omega}{\omega_c}\right)^{\frac{5}{12}}\right]\right\}\left(\frac{\omega}{\omega_c}\right)^{3/2} + \frac{4H_G}{CS_y}\left\{1-\exp\left[-\frac{1}{25}\left(\frac{\omega}{\omega_c}\right)^{\frac{5}{9}}\right]\right\}\frac{\omega}{\omega_c} \quad [9]$$

where

$$\frac{H_G}{S_y} = 2.84\left(1-\exp\left\{-0.82\left[\frac{\pi C e_y}{2}\sqrt{\frac{\omega}{\omega_c}}\left(\frac{\omega}{\omega_c \cdot \omega_t^*}\right)^{\frac{B}{2}}\right]^{-0.7}\right\}\right) \quad [10]$$

and the critical interference to cause initial yielding ω_c is derived independently of the hardness, to be:

$$\omega_c = \left(\frac{\pi \cdot C \cdot S_y}{2E'}\right)^2 R \quad [11]$$

where C is derived to be

$$C = 1.295\ \exp(0.736\nu) \quad [12]$$

This model then assumes that the individual asperity contact between rough surfaces can be approximated by hemispherical contact with a rigid flat. Then statistical relationships are used to model an entire surface of asperities with a range of heights described by a Gaussian distribution, $G(z)$. These statistical equations are given as:

$$P(d) = \eta A_n \int_d^\infty \bar{P}_F(z-d)G(z)dz \quad [13]$$

where the average spherical radius, R, at the tip of the asperities and the asperity surface density, η, are needed to model asperity contact using Eq. [23]. The distance between the surfaces can be described in two ways: (1) the distance between the mean of the surface heights, h, and (2) the distance between the mean of the surface asperities or peaks, d. These values of h and d are related by

$$h = d + y_s \quad [14]$$

The value of y_s is derived by Front *(14)* and given as:

$$y_s = \frac{0.045944}{\eta R} \quad [15]$$

where η is the area density of the asperities.

These values are approximated from profilometer measurements of δ and σ using the methods outlined in McCool *(15)*. The model provides an average contact force, P, as a function of surface separation or film thickness, h. In the numerical code, this relationship is used to predict the contact forces between the components of the thrust washer bearing. In the following sections the average contact force at a node i is assigned the notation F_{cont}^i such that $F_{\text{cont}}^i = P$.

Temperature/Viscosity Model

The lubricant viscosity is predicted by the Roelands equation, which models empirically the effects of temperature on viscosity (Roelands *(16)*). The pressure-independent form of Roelands equation is given as

$$\log(\log\mu + 1.2) = -S_o \log\left(1 + \frac{T_m}{135}\right) + \log(G_o) \quad [16]$$

Solving for the viscosity, μ, yields

$$\mu = \mu_\infty 10^{G_o(1+T_m/135)^{-S_o}} \quad [17]$$

where $\mu_\infty = 6.31 \times 10^{-5}$ N·s/m^2 and the rest of the variables can be found by fitting the formula to experimentally obtained viscosity values with respect to changing temperatures. This formula has been regressed to the measured viscosity of transmission fluid samples and found to be a good fit. For the transmission fluid used in this investigation $G_o = 3.545$ and $S_o = 1.053$.

Dry Friction Model

Locally, at the asperity contact, a simple friction model is used to calculate the sliding friction force caused by asperity contact. The test rig was run at low speeds under dry conditions and under nearly axisymmetric conditions to predict the friction coefficient for the dry contact. Certain conditions and materials behave in accordance to Amonton's law of friction, $F_{\text{frict}} = f \cdot F_{\text{cont}}$ where, in this case, F_{cont} is predicted from the asperity contact model. Although other materials do not follow this "law," as the friction coefficient, f may vary significantly with load. There are various fundamentally derived models of friction that also suggest this same phenomena, such as the works by Chang, et al. (*17*), Etsion and Amit (*18*), Chowdhury, et al. (*19*), and Kogut and Etsion (*20*). These works theorize that the plastic yielding of the contacting surface asperities can limit the COF between them. A regression of the data from the experimental test rig run dry or unlubricated resulted in the following empirical equation to model steel on steel friction:

$$f = 0.48 - 0.05\ln(F_{\text{cont}}) \quad [18]$$

Equation [18] may not be valid outside the range of the experimentally applied loads ($260.5N \le F_{\text{cont}} \le 1725.6N$).

Frictional Heating

This work models the friction at each point according to the asperity contact model and the fluid shear model. The entire friction force is assumed to be transferred to heat at the contact point according to the equation at node i

$$q_{\text{friction}}^i = F_i V_i \quad [19]$$

where F_i is the average friction force and V_i is the relative sliding speed at the node. The average friction force is calculated from the asperity contact model. The viscous shearing of the lubricant also generates heat at the node. The equation for the viscous heating at an element e is written as

$$q_{\text{viscous}}^i = \int_e \left(\mu \frac{V^2}{h}\right) dA_e \quad [20]$$

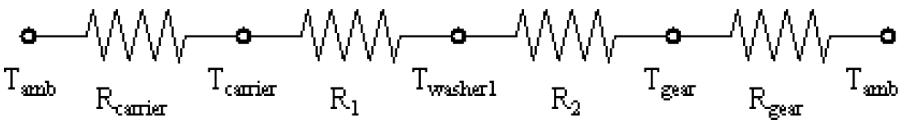

Fig. 2—Schematic of main components of the tested thrust washer bearing.

where μ is the effective viscosity, V is the relative speed between the surfaces, h is the film thickness, and A_e is the area of a given element e.

If the relative speed between the two surfaces is large enough, each point on the surface will essentially see an average heat generation of all nodes that are the same distance from the axis of rotation. This is because heat propagation is a time-dependent process that is relatively slow in comparison to the rotational speed of most mechanical devices. Essentially, the temperature profile of washers that are rotating relative to neighboring components will be approximately axisymmetric. However, certain components may be stationary, like the carriers or washers that stick to neighboring components due to friction. The above approximation is then no longer valid, but the heat generation then becomes stationary and so it can be easily applied as nodal boundary conditions.

Heat Balance

The finite difference technique is used to solve the steady-state heat conduction problem. Each component is modeled as a 2-D annulus with heat conduction and generation occurring between their contacting points. The two-dimensional steady-state heat transfer equation using cylindrical coordinates r and θ is:

$$\frac{\partial^2 T}{\partial r^2} + \frac{1}{r}\frac{\partial T}{\partial r} + \frac{1}{r^2}\frac{\partial^2 T}{\partial \theta^2} + \frac{1}{k}Q(r,\theta) \qquad [21]$$

where $Q(r,\theta)$ is volumetric heat generation, T is the periodic temperature distribution around the circumference, and

$$r = \sqrt{x^2 + y^2} \qquad [22]$$

$$\theta = \tan^{-1}\left(\frac{y}{x}\right) \qquad [23]$$

Heat transfer is thus considered through the x and y plane of each component. Each component is meshed using a uniform cylindrical coordinate system and Eq. [21] is then discretized using the finite difference method. The finite difference discretized heat transfer equations in cylindrical coordinates from Özisik *(21)* pgs. 469-471 are used.

The mesh used to discretize the modified Reynolds equation (Eq. [1]) coincides with the mesh used to discretize Eq [21]. At each nodal location, the volumetric heat is the sum of the heat conducted to or from adjacent points on the bearing components (q_{cond}) and the heat generated due to friction (Eq. [19]) and viscous shearing (Eq. 20):

$$Q(r,\theta) = (q_{\text{cond}} + q_{\text{friction}} + q_{\text{viscous}})_i / t_i \qquad [24]$$

where t_i is the thickness of the component at node i. The heat transferred through to each node from adjacent components (q_{cond}) is modeled as a one-dimensional conduction problem as described in the following paragraphs. At the inner and outer radii, the boundary condition of a zero heat flux is assumed. Thus, heat convection is not considered because it is assumed to be small in comparison to the heat conduction.

The heat flowing away from the surfaces of the carrier and the gear are assumed to occur only due to one-dimensional conduction along the z-axis toward an ambient temperature set within the components. The ambient temperature is set to an approximate room temperature of 24°C. The heat transfer between the components is modeled as one-dimensional conduction in the z-direction (see Fig. 2). Thus, conduction between the components (but not within each component) is considered only between nodes at the same radial and circumferential location. Using the equivalent thermal resistance between each component at each nodal location, a prediction for the path of the heat conducted between the components is made. The thermal resistances between the components is calculated by

$$R_{\text{carrier}} = \frac{t_{\text{carrier}}}{K_{\text{carrier}}} \qquad [25]$$

$$R_1 = R_{\text{fluid}} + \frac{R_{\text{washer1}}}{2} = \frac{h}{K_{\text{atf}}} + \frac{t_{\text{washer1}}}{2K_{\text{washer1}}} \qquad [26]$$

$$R_2 = R_{\text{fluid}} + \frac{R_{\text{washer1}}}{2} = \frac{h}{K_{\text{atf}}} + \frac{t_{\text{washer1}}}{2K_{\text{washer1}}} \qquad [27]$$

$$R_{\text{gear}} = \frac{t_{\text{gear}}}{K_{\text{gear}}} \qquad [28]$$

where t is the thickness of the component in subscript and K is the thermal conductivity. Then the one-dimensional heat conduction from a point a on one component to a point b on an adjacent component along the z-axis is calculated as

$$q_{\text{cond}} = \frac{(T_a - T_b)}{R_{a\to b}} \qquad [29]$$

Equation [29] is substituted into Eq. [24] to calculate the total volumetric heat at a node. The Gauss-Seidel method is used to solve for the temperature from the finite difference discretized equations. The temperature of two adjacent nodes on two sliding surfaces is also averaged to approximate the fluid temperature, T_m. Then T_m is substituted into Eq. [17] to calculate the fluid viscosity at that node.

Force and Moment Calculations

The force balance of the individual components of the washer bearing (washer, carrier, gear) will each be solved individually using their specified boundary conditions. The elasto-plastic asperity contact model calculates the average contact force, F^i_{cont}, at each node on the surfaces between the components. The solution of the modified Reynolds equation (Eq. [1]) solves for the fluid pressures, which are integrated to provide the fluid force at each node, F^i_{fluid} using Eq. [7]. At each surface node i the total force is calculated as:

$$F^i = \left(F^i_{\text{cont}} + F^i_{\text{fluid}}\right) \qquad [30]$$

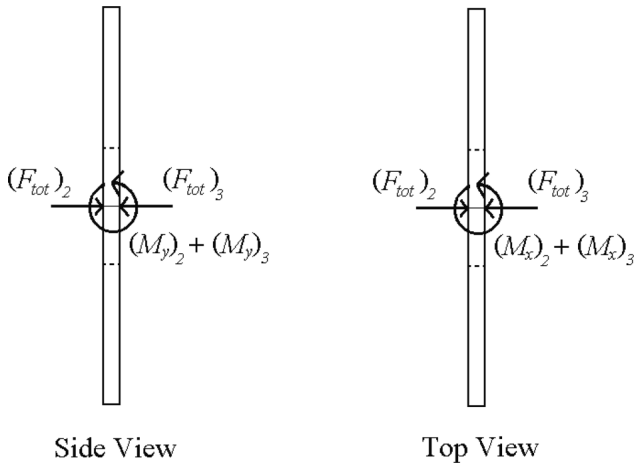

Fig. 3—Free body diagram of washer.

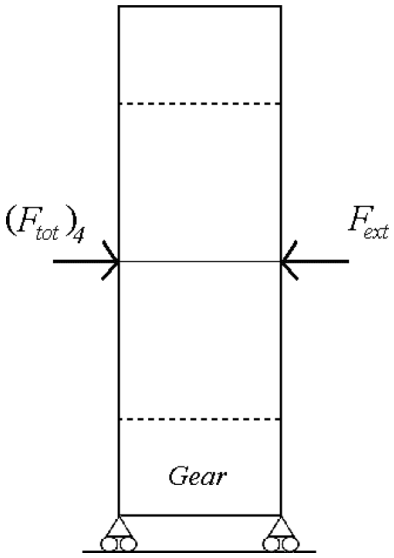

Fig. 4—Free body diagram of gear.

A force and moment balance is performed by summing the contact forces and fluid forces of each component. Between each component there will be forces due to contact, fluid pressures, or an externally applied load. For a bearing consisting of a carrier, washer and gear there are four surfaces (see Fig. 1). On each surface the axial load and moments are calculated as:

$$(F_{\text{tot}})_n = \left(\sum_{i=1}^{i_{\text{total}}} F^i \right)_n \quad [31]$$

$$(M_x)_n = \left(\sum_{i=1}^{i_{\text{total}}} F^i y^i \right)_n \quad [32]$$

$$(M_y)_n = -\left(\sum_{i=1}^{i_{\text{total}}} F^i x^i \right)_n \quad [33]$$

where n is the surface number (the surfaces are numbered from 1 to 4 from left to right in Fig. 1 so that the surface of the carrier is surface 1 and the surface of the gear is surface 4) and i_{total} is the total number of nodes on each surface. Figure 3 shows the resulting free body diagram of the washer.

As is represented in Fig. 3, for the washer, the total force and moment balance are given by:

$$(F_{\text{tot}})_2 + (F_{\text{tot}})_3 = 0 \quad [34]$$

$$(M_x)_2 + (M_x)_3 = 0 \quad [35]$$

$$(M_y)_2 + (M_y)_3 = 0 \quad [36]$$

For the gear, the moments are not shown because the gear is not free to rotate and so only the axial load must be balanced. The free body diagram for the gear is shown in Fig. 4. The total force balance is given by the equation:

$$(F_{\text{tot}})_4 + F_{\text{ext}} = 0 \quad [37]$$

The force and moment balance depend ultimately on the location and orientation of the washers and gear. Thus the problem is formulated as a nonlinear set of 4 equations (Eqs. [34-37]) with 4 unknowns. These equations are dependent on the governing physical equations of the thrust washer bearing and consider asperity contact, boundary, and full-film lubrication; and heat generation and balance. The unknowns are the axial location of each component, z, and the tilt of each component about the x- and y-axis, γ_x and γ_y (see Fig. 1). The gear is able to translate in the z direction, but has a fixed tilt, γ_{tilt}, about the y-axis and so accounts for one degree of freedom. The washer is able to tilt about the x- and y-axis and also move along the z-axis and so has three degrees of freedom. The four unknowns are explicitly z_w, z_g, $(\gamma_x)_w$, *and* $(\gamma_y)_w$.

Integrated Numerical Scheme and Convergence

The above methods are coupled through their boundary conditions and so they must be satisfied simultaneously. This will be done by use of an iterative process. The Newton-Raphson method solves the set of nonlinear equations (Eq. [34-37]) resulting from the coupled thrust washer bearing model. Since the derivatives of these nonlinear equations cannot be solved for analytically, the centered finite-difference method is used to approximate them.

$$f'(x_i) = \frac{-f(x_{i+2}) + 8f(x_{i+1}) - 8f(x_{i-1}) + f(x_{i-2})}{12\Delta x} \quad [38]$$

where f is one of the unbalanced sums of the force and moment balances (Eqs. [34-37]) and x represents one of the four unknown variables (z_w, z_g, $(\gamma_x)_w$, or $(\gamma_y)_w$).

The flow chart shown in Fig. 5 depicts the overall iterative procedure and how the solution is checked for convergence. The interfacial conditions between the components, such as fluid pressure and contact force, are adjusted via the Newton-Raphson technique until they converge to the final solution. Initially, the contact forces and fluid pressures are set to zero. The bearing components are initially evenly spaced and the minimum film thickness between them is set to $h_{\min}/\sigma = 3$. The initial temperature throughout the bearing is set to the ambient temperature. The overall boundary conditions are also set at the same time (at the inner and outer radius, $p = 0$). The flow chart also indicates that once the model converges, output values such as frictional torque and hydrodynamic load support are calculated (see the following sections).

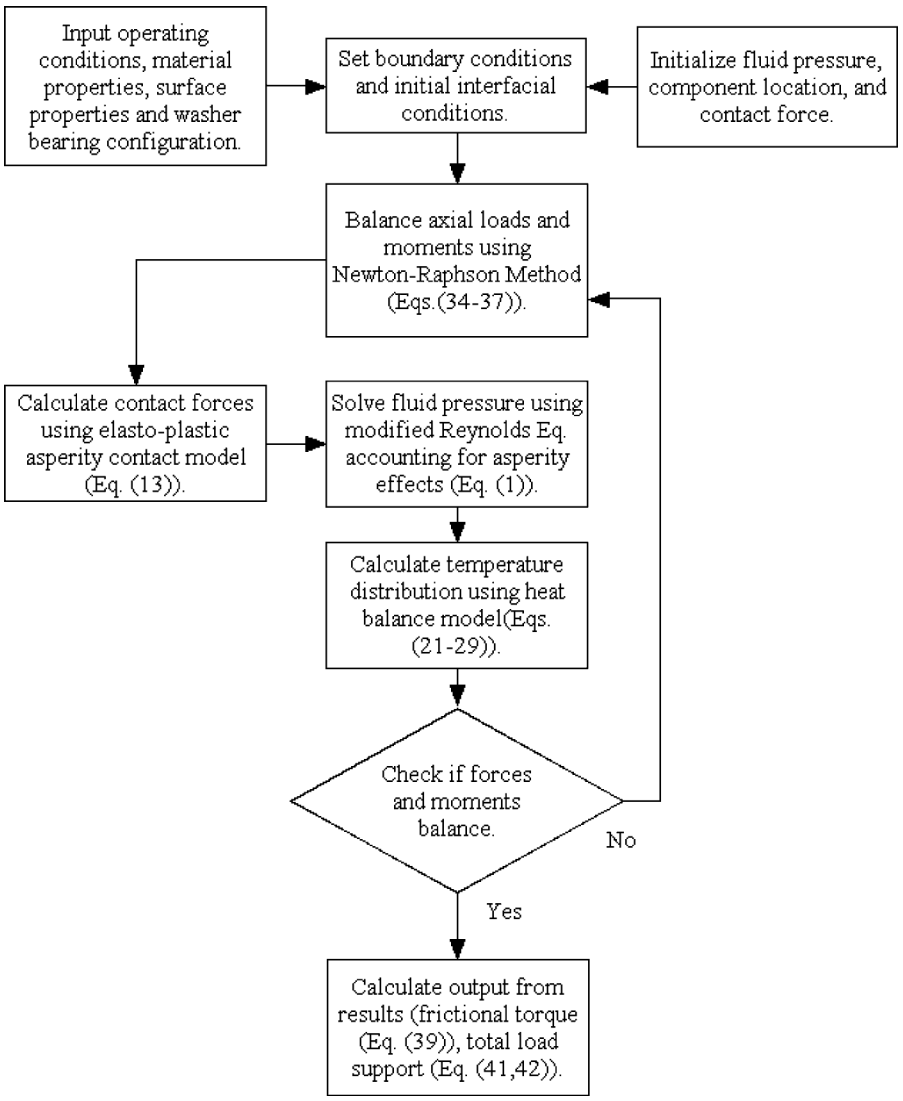

Fig. 5—Flow chart representation of algorithm to model a thrust washer bearing.

Frictional Torque

The frictional torque is calculated about the z-axis by summing the torques resulting from each frictional force at each node i on the surface of the bearing. The resulting equation for frictional torque on surface n is

$$(T_{\text{frict}})_n = \sum_n \left[\left(F^i_{\text{frict}} + F^i_{\text{viscous}} \right) \cdot r \right]_i \qquad [39]$$

where F_{viscous} is the force due to viscous shearing on the bearing surface and is given by

$$F^i_{\text{viscous}} = \int_i \left(\mu \frac{V}{h} \right) dA_i \qquad [40]$$

where V is the relative speed between the surfaces and A_i is the area surrounding node i. The lowest total frictional torque between the six bearing surfaces is assumed to be the overall frictional torque, which is transferred through the bearing.

Hydrodynamic Load Support

The total load carried by hydrodynamic lift is calculated by summing the nodal fluid forces of Eq. [7] on surface n:

$$(F_{\text{fluid}})_n = \left(\sum_{i=1}^{i_{\text{total}}} F^i_{\text{fluid}} \right)_n \qquad [41]$$

The total load carried by asperity contact is also calculated by summing the average contact force at each node given in Eq. [13]:

$$(F_{\text{cont}})_n = \left(\sum_{i=1}^{i_{\text{total}}} F^i_{\text{cont}} \right)_n \qquad [42]$$

Stop Criteria

As the temperature increases, eventually the lubricant viscosity drops enough that the hydrodynamic lift is insufficient to separate the surfaces. Then asperity contact occurs and the friction increases even more, causing the viscosity to decrease and the film to collapse quickly. This occurrence is labeled here as

TABLE 1—GEOMETRY AND MATERIAL PROPERTY INPUTS

:	Oil	Carrier	Washer	Gear
I.D.	—	—	0.0111 m	0.0156 m
O.D.	—	—	0.0227 m	0.0227 m
Thickness (t)	—	0.01 m	6.35E-4 m	0.01 m
γ_{tilt}	—	0 rad	—	0.002 rad
δ		4.50E-07 m	4.50E-07 m	4.50E-07 m
σ	—	5.15E-07 m	5.15E-07 m	5.15E-07 m
E	—	201 GPa	201 GPa	201 GPa
S_y	—	0.993 GPa	0.993 GPa	0.993 GPa
ν	—	0.296	0.296	0.296
α	—	1.2E-05/°C	1.2E-05/°C	1.2E-05/°C
K	0.145 W/m · K	60.5 W/m · K	60.5 W/m · K	60.5 W/m · K
S_o	1.053	—	—	—
G_o	3.545	—	—	—

thermo-viscous distress (TVD). Due to the phenomenon of TVD the computer simulation may diverge, stall, or run in an infinite loop if not tracked properly. For this reason, a few criteria are used to abort a load step prior to any numerical problems occurring. The criteria that have proven effective are:

1. If the bearing reaches an average temperature 200°C greater than ambient temperature.
2. If the temperature gradient continues to increase after a set number of iterations.

RESULTS

The numerical thrust washer bearing simulation is used to map and quantify the effect of various parameters on washer bearing performance. The case of a single round steel washer is considered in this work. The numerical program takes about 30 min to run an initial load step on a 1.8-Ghz PC. Once the initial load step is reached it takes considerably less time to converge to a new load step.

A tilt of γ_{tilt} is imposed on the gear to simulate the loading conditions in the transmission mimicking a moment that causes the gear to tilt. The tilt is applied to simplify the problem and allow for a faster time until convergence. For the case of a single steel washer, the geometry and material properties found in Table 1 are used. These properties are based on the experimental set-up and the conditions seen in an actual automatic transmission. The relative velocity is applied between the washer and the carrier (see section on component rotational speed).

Since the macro-scale deformations are neglected, the components behave rigidly, but pressures due to the elasto-plastic asperity contact are still produced. The contacts will thus be very concentrated and the contact pressures very high. This also results in a small contact area, which increases the thermal resistance between components, thus increasing temperatures in the bearing. Certain mechanisms that control bearing behavior are still present, and their effect on bearing performance can be quantified.

Figure 6 shows the rigid bearing results for the effective coefficient of friction as a function of load and speed. Jackson and Green (*1*) contains a short derivation of the formula used in calculating the effective coefficient of friction from the frictional torque. The formula is given below:

$$f_{\text{eff}} = \frac{3}{2} \cdot \frac{T_{\text{frict}}(r_o^2 - r_i^2)}{F_a(r_o^3 - r_i^3)} \qquad [43]$$

where

f_{eff}– effective coefficient of friction
F_a– axial load, [N]
T_{frict}– frictional torque (from Eq. [39]), [N · m]
r_i– inner diameter of washer, [m]
r_o– outer diameter of washer, [m]

As shown in Fig. 6, at the lowest speed of 136 rad/s, the bearing does not produce enough hydrodynamic lift to separate the components, and the resulting effective coefficient of friction is in the range of asperity contact. At the higher speeds, the effective

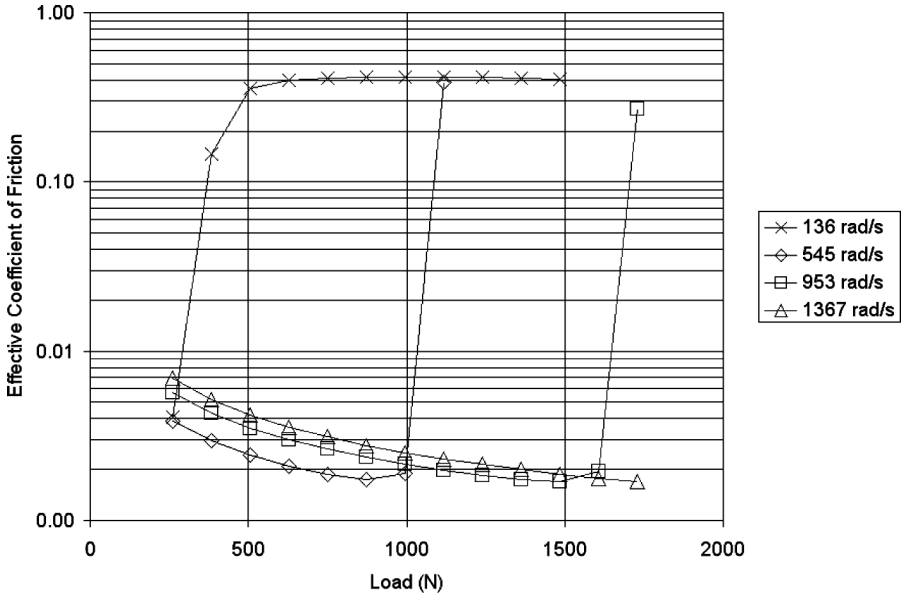

Fig. 6—The effective coefficient of friction plotted as a function of load and speed ($\gamma_{tilt} = 0.002$ rad).

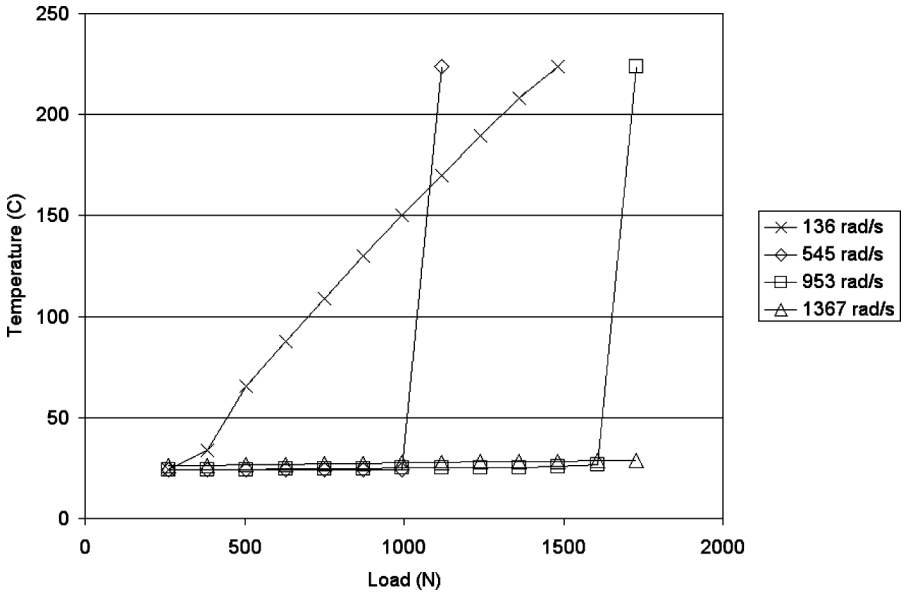

Fig. 7—The average bearing temperature plotted as a function of load and speed.

coefficient of friction is much lower and in the typical range of full-film lubrication. Even at these higher speeds, eventually, higher loads will overcome the hydrodynamic lift and TVD occurs. The points of distress are marked by sharp increases in the effective coefficient of friction. This sudden distress is a real phenomenon, which also occurs during the experimental portion of this investigation and in Jackson and Green (*1*).

Figure 7 shows that the average bearing temperature remains near the ambient temperature, while full-film lubrication is maintained. However, once the load overcomes the hydrodynamic lift, the temperature increases drastically due to TVD. At the lowest speed it appears that TVD does not occur immediately, rather, the temperature gradually increases with load as the hydrodynamic lift is slowly overcome.

The minimum film thickness, $h_{\min}$, decreases with load for all speeds (see Fig. 8). The magnitude of the film thickness gradient also decreases with load, indicating an increasing effective stiffness of the asperity contact and fluid film. This trend is broken when bearing distress occurs and the film thickness decreases drastically for 545 rad/s at 1117 N and for 953 rad/s at 1728 N. This decrease in film thickness is also due to TVD.

Since the hydrodynamic moment is out of phase with the tilt imposed on the gear about the *y*-axis, it causes the washer to tilt about the *x*-axis (see Fig. 9). At low speed, where the hydrodynamic

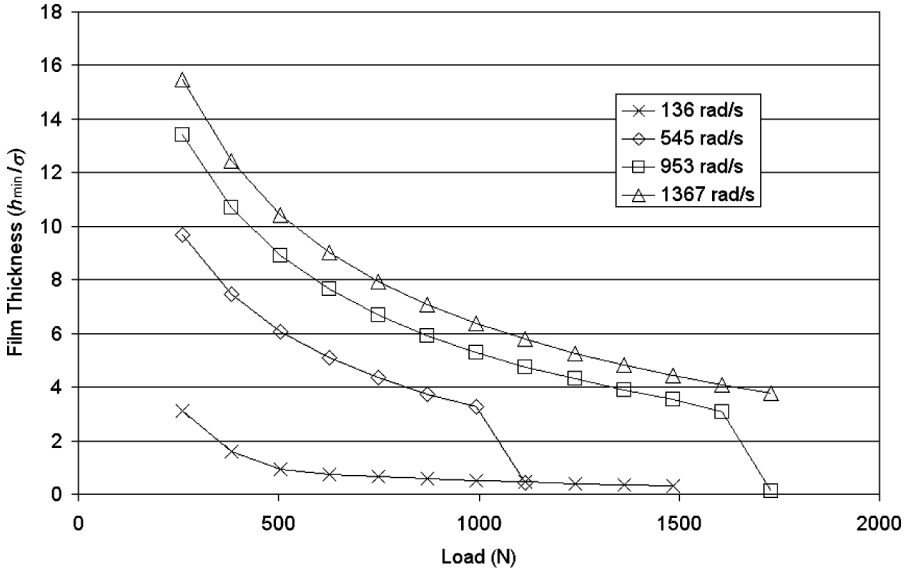

Fig. 8—The normalized minimum film thickness plotted as a function of load and speed.

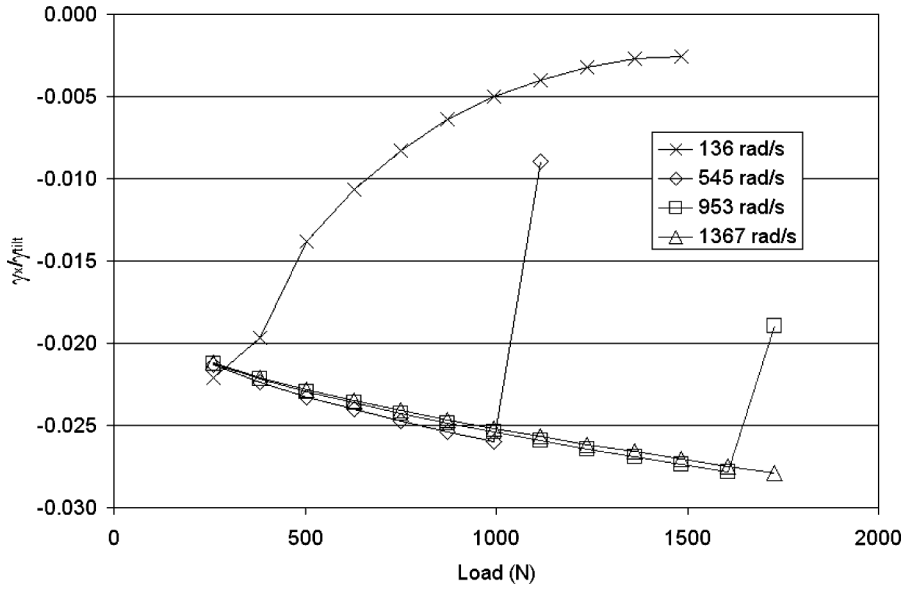

Fig. 9—The normalized washer tilt about the *x*-axis plotted as a function of load and speed.

lift cannot separate the components, $\gamma_x/\gamma_{\text{tilt}}$ approaches the static case of zero with increasing load. For rotational speeds 545 rad/s, 953 rad/s, and 1367 rad/s, the hydrodynamic lift increases to match the increasing load, and $\gamma_x/\gamma_{\text{tilt}}$ also increases. When the hydrodynamic lift is overcome by the applied load due to TVD, the magnitude of $\gamma_x/\gamma_{\text{tilt}}$ decreases drastically.

When sufficient, the hydrodynamic lift pushes the washer against the tilted gear (see Fig. 10). Thus, for high speeds and low loads, $\gamma_y/\gamma_{\text{tilt}}$ approaches the value of one. Once the applied load begins to overcome the hydrodynamic lift, $\gamma_y/\gamma_{\text{tilt}}$ decreases toward a value of 0.5, which corresponds to the static position of the washer. This is the static position of the washer because, for the moments to balance the contact pressure distribution on both sides of the washer must be a mirror image of each other. For the speeds shown above 136 rad/s, $\gamma_y/\gamma_{\text{tilt}}$ drastically changes due to the fluid film succumbing to TVD, while for the slowest speed of 136 rad/s the shift in the $\gamma_y/\gamma_{\text{tilt}}$ is a gradual one.

Since the tilts about the x- and y-axis are very small, an equivalent nutation tilt, γ_n, vector can be found that results in the same washer orientation. Since γ_y is much larger than γ_x, the equivalent nutation angle γ_n is practically identical to γ_n. In vector form, this relationship is:

$$\vec{\gamma}_n = \vec{\gamma}_x + \vec{\gamma}_y \qquad [44]$$

Although some tilt does occur about the x-axis due to hydrodynamic lift, most of the tilt of the washers occurs about the y-axis,

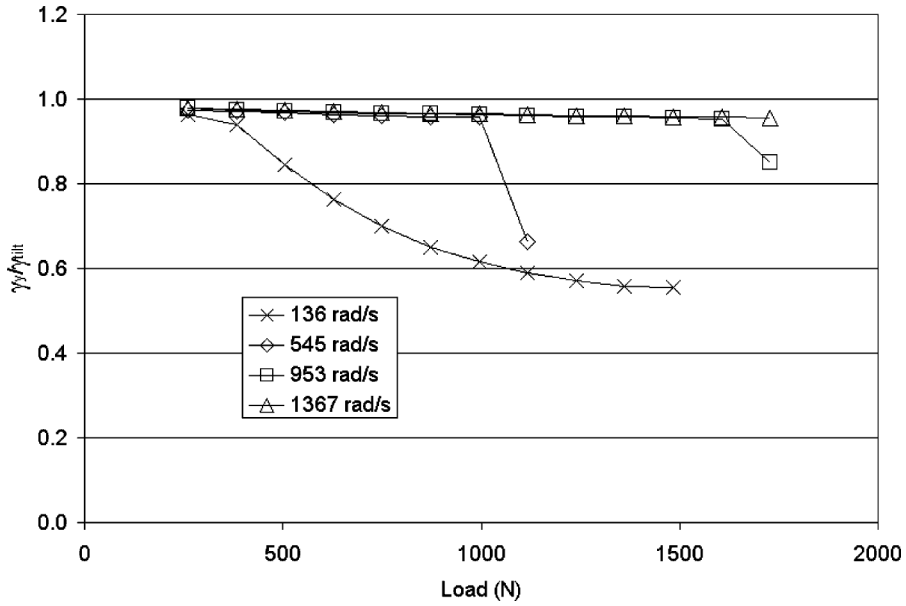

Fig. 10—The normalized washer tilt about the *y*-axis plotted as a function of load and speed.

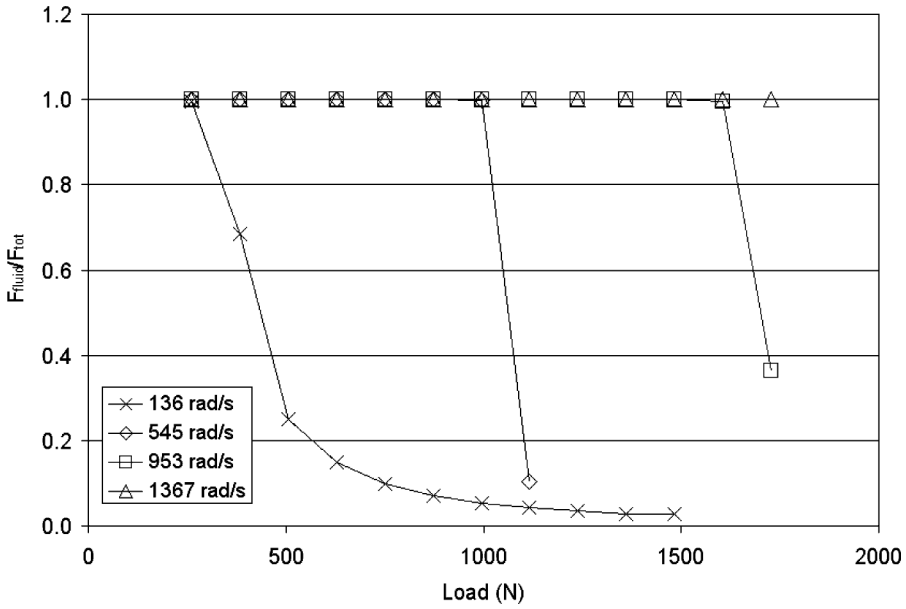

Fig. 11—The normalized hydrodynamic lift about the *x*-axis plotted as a function of load and speed.

about which the tilt on the gear is applied. It appears that the presence of hydrodynamic lift will slightly increase the overall tilt of the washer. This could have a positive effect in that a larger tilt may increase hydrodynamic lift, and a negative effect because the concentrated area of contact is smaller (resulting in higher contact pressure and heat generation).

In Fig. 11 the normalized hydrodynamic lift, $F_{\text{fluid}}/F_{\text{tot}}$, is plotted versus load and speed. At the lowest speed of 136 rad/s, sufficient hydrodynamic lift is not generated and the total applied load is carried by both asperity contact and hydrodynamic lift. As load is increased at 136 rad/s, proportionally more of the load is carried by asperity contact. At 1361 N and 136 rad/s, approximately 2% of load is being carried by hydrodynamic lift. For 545 rad/s, 953 rad/s, and 1367 rad/s, the hydrodynamic lift carries the entire load until TVD is reached at which the hydrodynamic lift drops dramatically.

The asperity contact force is plotted logarithmically with respect to load and speed in Fig. 12. Even at apparently fully hydrodynamic lift there is slight asperity contact, although the load carried by the asperities can be many orders of magnitude smaller than the hydrodynamic lift. This suggests, though, that even when a nearly full-film of lubrication separates the bearings, very small

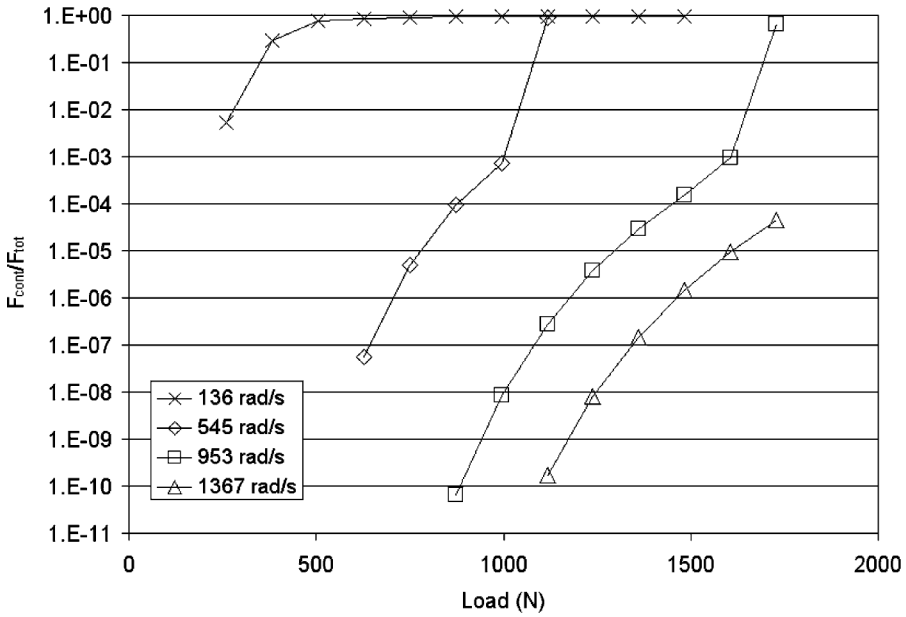

Fig. 12—The normalized contact load as a function of applied load and speed.

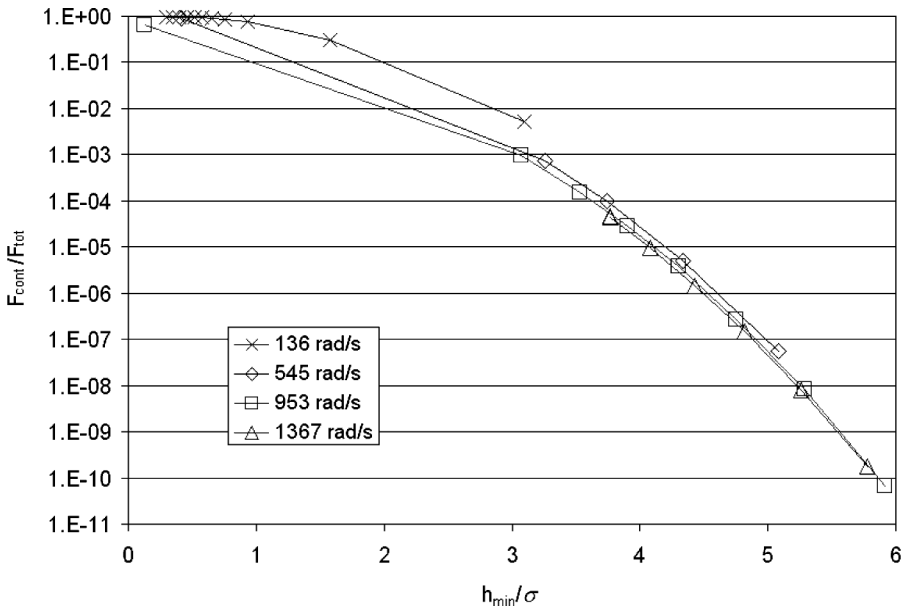

Fig. 13—Plot of normalized contact load as a function of the normalized minimum film height.

amounts of contact can occur. As load is increased, the load carried by asperity contact increases until a distress point causes the hydrodynamic lift to effectively disappear, leaving the asperities to carry the entire load.

Figure 13 shows the normalized contact load, F_{cont}/F_{tot}, plotted as a function of the normalized minimum film height, h_{min}/σ, and speed. It is clear that the contact force increases sharply as the minimum film height decreases. At $h_{min}/\sigma \approx 3$, commonly used to mark the threshold of significant asperity contact, F_{cont}/F_{tot} jumps quickly to points near $F_{cont}/F_{tot} = 1$. This represents the collapse of the fluid film thickness due TVD. Washer bearings intended to operate at high speeds should be designed to generate enough lift to sustain $h_{min}/\sigma > 3$. It should be noted that even though the numerical simulation predicts when asperity contact will become significant, wear is not modeled.

At the lowest speed of 136 rad/s it appears the thermo-viscous distress is not as severe, probably since less kinetic energy is available to dissipate in the form of frictional heat (see Fig. 13). This illustrates that at low speeds the bearing operates in the mixed and boundary lubrication region and at high speeds in the full-film lubrication region unless the load is great enough to cause TVD and collapse the film.

Figure 14 shows a plot of the numerically generated data in the form of a Stribeck curve (the traditional Stribeck notation

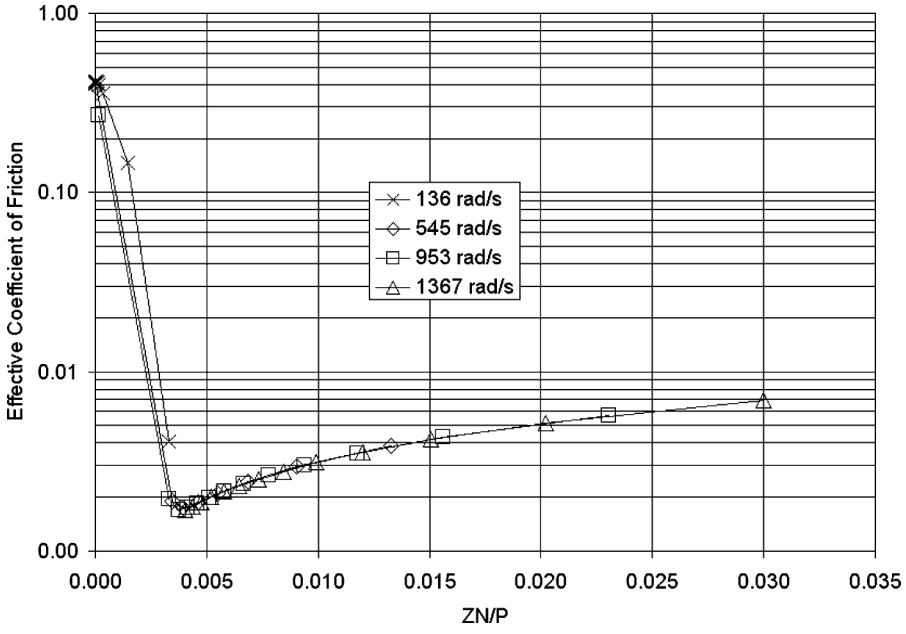

Fig. 14—Stribeck curve generated from numerical results.

ZN/P is used). The different regimes of bearing lubrication are clearly represented here. For higher Stribeck numbers, the bearing operates in the full-film region (to the right of the "knee"). Moving to the left, the friction coefficient decreases until the bearing's point of optimal efficiency is reached at a *ZN/P* value of about 2.0E-6. In the experimental results this value is about 1.0E-6. Then, as the Stribeck value is further decreased, the bearing enters the mixed lubrication regime. At this point, high speeds will cause the bearing to heat quickly and experience thermo-viscous distress. With distress, the fluid film collapses and the friction coefficient rises dramatically. However, at low speeds, the process is more gradual and the film does not collapse immediately.

Component Rotational Speed

The round thrust washers in the transmission and test rig are allowed to rotate about the shaft and the axis of symmetry. The steady-state rotational speed of each washer will thus depend on initial conditions and the dynamics that occur during start-up before steady-state is reached. However, in the numerical code, the rotational speed of each component is assigned manually and held constant. This work assumes that the washer speeds will adjust to the optimal configuration, resulting in the minimal amount of frictional loss. What will most likely result is that the washers will stick to either the gear or carrier and the entire relative speed will be carried between only two components. Once this situation occurs, the washers are essentially "stuck" because the friction between the sliding surfaces is usually much less than the static surfaces due to hydrodynamic lift. In other words, the frictional torque of the sliding surfaces cannot overcome the static frictional torque to "free" the washer from the component it is stuck to. Experimental observations of wear confirm that most of the relative speed is carried between two components.

For this work, it is assumed that the bearing will run at the rotational speed configuration that produces the lowest frictional torque. By modeling the bearing with the speed being taken at different surfaces, this "optimal" configuration is predicted. The numerical results suggest that the washers provide more hydrodynamic lift by increasing the bearing surface area in comparison to just the gear. By the washer sticking to the gear, the bearing surface is increased by 31%. This allows for more hydrodynamic lift to develop. The washer may also have other positive effects through its deformation and changing the angle of tilt between the sliding surfaces.

Effect of Dry Friction Coefficient

The dry friction coefficient, f, is varied to show the effect it has on bearing performance and distress. Reducing the dry coefficient of friction not only decreases the effective coefficient of friction for the bearing, but also decreases the frictional heat generated.

As expected, changes in the dry friction coefficient only affect the left side of the numerically generated Stribeck curve (see Fig. 15). As must be the case, the dry friction coefficient does not alter the effective coefficient of friction while the bearing is operating with a full film of lubrication separating the surfaces. It is also evident that increasing the friction shifts the point of TVD to lower loads. The dry coefficient of friction merely shifts the initiation of boundary lubrication (the valley in the curve) to larger Stribeck values (farther to the right). Thus, increasing the dry coefficient of friction reduces the range of operational conditions that the bearing can operate within the mixed lubrication regime. These findings suggest that lower dry friction coefficients between thrust washer bearing components will improve bearing performance. This is also confirmed by the experimental results of the washers coated with low-friction PTFE in Jackson and Green (*2*).

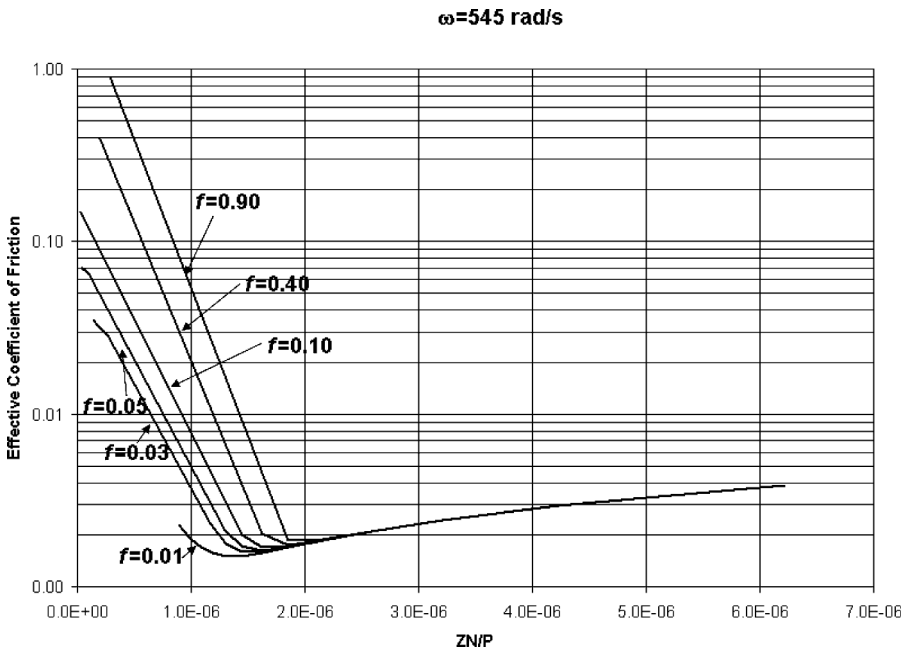

Fig. 15—The numerically generated Stribeck plot for varying dry friction coefficients.

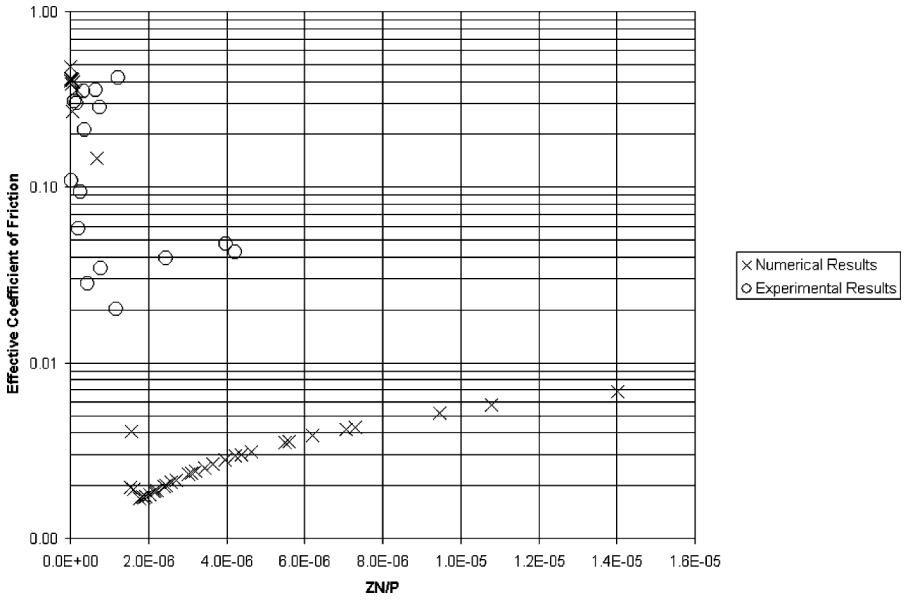

Fig. 16—Comparison of experimentally and numerically generated thrust washer bearing Stribeck curves.

Comparison to Experimental Results

Figure 16 compares the Stribeck curves generated from the numerical and experimental results for the same loads, speeds, geometry, and materials as the numerical study. Although the experimental and numerical results both produce a Stribeck curve, the quantitative values of the curves differ significantly. An ideally designed thrust bearing will operate in the full-film lubrication regime on the right of the Stribeck curve. If the bearing operates in this region, it will have little wear and low friction. Also, the numerically and experimentally predicted critical points of the Stribeck curve, at the initiation of mixed lubrication on the left side of the curve, are offset from each other. The numerical simulation makes a number of assumptions that may account for large differences between the numerical and experimental results. The most notable of these assumptions is that wear is not modeled or considered. In an actual bearing application, wear will affect the performance in a number of different ways. Wear will alter the geometry and roughness of the bearing surfaces. Altering the geometry will affect the hydrodynamic lubrication and the friction between the surfaces, and thus has the potential to cause large differences between the numerical and experimental results.

Since there should be no wear and contact in the full-film regime (on the right side of the Stribeck curve), the numerical and experimental friction coefficient should be more likely to agree. However, this is not the case. The experimental results predict an effective friction coefficient that is higher on the right side of the Stribeck curve than the numerical results. There are a number of possibilities that may explain this: (1) Contact is occurring due to imperfections in the washer surface such as "very high" asperity peaks that are not accounted for in the numerical model. (2) Waviness in the washers affects the lubrication and contact between the bearing surfaces. (3) Wear occurring during start-up (before the bearing reaches the full-film regime) changes the bearing geometry. (4) Vibrations in the test rig cause the bearing surfaces to contact periodically, despite sufficient hydrodynamic lift. It seems very likely that vibrations and imperfections of the bearing geometry could cause contact to occur even when the hydrodynamic lift might be sufficient to provide a full film of lubrication for ideal conditions. Ball bearing rotation, meshing of the gear teeth, and the excitation of the inherent natural frequencies of the system may account for such vibrations occurring in the test rig.

CONCLUSIONS

By considering heat generation and thermo-viscous effects, the numerical solution captures the physical mechanism of TVD. This mechanism is believed to be a possible cause of severe and sudden distress in the bearing during operation.

The numerical model generates the traditional trends of the Stribeck curve when plotted. The numerical model thus predicts that the washer can operate in all the regions of the Stribeck curve (full-film lubrication, mixed lubrication, and boundary lubrication). However, once asperity contact occurs in the mixed and boundary lubrication regimes, the friction increases significantly and the bearing becomes much more likely to distress due to TVD.

The dry friction coefficient was varied to investigate the effect it has on bearing behavior. Decreasing the friction coefficient significantly improves the range of effective bearing behavior. By decreasing the dry friction, the frictional heat generation also decreases significantly. This is effective at expanding the loads and speeds that the bearing can operate at without TVD occurring.

Next the experimental methodology was outlined and the results are compared to the numerical results. The trend of the Stribeck curve predicted by the numerical code are confirmed in the experimental results. Although in many cases the numerical and experimental results do not quantitatively agree, it is most important that they predict some of the same qualitative trends in bearing behavior.

ACKNOWLEDGEMENTS

This research was funded by General Motors through the Center for Surface Engineering and Tribology. Mr. David Zini is the program manager. This support is gratefully acknowledged.

REFERENCES

(1) Jackson, R. L. and Green, I. (2001), "Study of the Tribological Behavior of a Thrust Washer Bearing," *Trib. Trans.,* **44**(3), pp 504-508.

(2) Jackson, R. L. and Green, I. (2003), "Experimental Analysis of the Wear, Life and Behavior of PTFE Coated Thrust Washer Bearings under Non-axisymmetric Loading," *Trib. Trans.,* **46**(4), pp 600-607.

(3) Cameron, A. and Wood, W. L. (1958), "Parallel Surface Thrust Bearing," *ASLE Trans.*, **1**, pp 254-258.

(4) Kazama, T. and Yamaguchi, A. (1993), "Application of a Mixed Lubrication Model for Hydrostatic Thrust Bearings of Hydraulic Equipment," *ASME J. Tribol.*, **115**, pp 686-691.

(5) Patir, N. and Cheng, H. S. (1978), "An Average Flow Model for Determining Effects of Three-Dimensional Roughness on Partial Hydrodynamic Lubrication," *ASME J. Tribol.*, **100**, pp 12-17.

(6) Patir, N. and Cheng, H. S. (1979), "Application of Average Flow Model to Lubrication Between Rough Sliding Surfaces," *ASME J. Tribol.*, **101**, pp 220-230.

(7) Yu, T. and Sadeghi, F. (2001), "Groove Effects on Thrust Washer Lubrication," *ASME J. Tribol.*, **123**(1), pp 295-304.

(8) Yu, T. and Sadeghi, F. (2002), "Thermal Effects in Thrust Washer Lubrication," *ASME J. Tribol.*, **123**(1), pp 166-177.

(9) Kucinschi, B. R., DeWitt, K. J. and Pascovici, M. D. (2004), "Thermoelastohydrodynamic (TEHD) Analysis of a Grooved Thrust Washer," *ASME J. Tribol.*, **126**, pp 267-274.

(10) Reddy, J. N. (1993), "An Introduction to the Finite Element Method," 2nd Ed., Mcgraw-Hill, New York.

(11) Jackson, R. L. and Green, I. (2004), "A Finite Element Study of Elasto-Plastic Hemispherical Contact," *ASME J. Tribol.,* **127**(2), pp 343-354.

(12) Jackson, R. L. and Green, I., "A Statistical Model of Elasto-Plastic Asperity Contact of Rough Surfaces," *Proc. of the 2003 ASME/STLE International Tribology Conference, Preprint 2003-TRIB268.*

(13) Quicksall, J., Jackson, R. L. and Green, I. "Elasto-Plastic Hemispherical Contact for Varying Mechanical Properties," *IMechE J. of Eng. Trib.—Part J,* 218, pp 313-322.

(14) Front, I. (1990), "The Effects of Closing Force and Surface Roughness on Leakage in Radial Face Seals," MS Thesis, Technion, Israel Institute of Technology.

(15) McCool, J. I. (1986), "Comparison of Models for the Contact of Rough Surfaces," *Wear*, **107**, pp 37-60.

(16) Roelands, C. J. A. (1966), "Correlational Aspects of the Viscosity-Temperature-Pressure Relationship of Lubricating Oils. Druk," V. R. B., Groingen, Netherlands.

(17) Chang, W. R., Etsion, I. and Bogy, D. B. (1988), "Static Friction Coefficient Model for Metallic Rough Surfaces," *ASME J. Tribol.*, **110**, pp 57-63.

(18) Etsion, I. and Amit, M. (1993), "The Effect of Small Normal Loads on the Static Friction Coefficient for Very Smooth Surfaces," *ASME J. Tribol.*, **115**, pp 406-410.

(19) Roy Chowdhury, S. K. and Ghosh, P. (1994), "Adhesion and Adhesional Friction at the Contact Between Solids," *Wear,* **174**, pp 9-19.

(20) Kogut, L. and Etsion, I. (2003), "A Semi-Analytical Solution for the Sliding Inception of a Spherical Contact," *ASME J. Tribol,* **125**(3), pp 499-506.

(21) Özisik, M. N. (1993), *Heat Conduction*, 2nd Ed., John Wiley, New York.